

Photo-disintegration cross section measurements on ^{186}W , ^{187}Re and ^{188}Os : implications to the Re-Os cosmochronology

T. Shizuma¹, H. Utsunomiya², P. Mohr³, T. Hayakawa¹, S. Goko², A. Makinaga², H. Akimune², T. Yamagata², M. Ohta², H. Ohgaki⁴, Y.-W. Lui⁵, H. Toyokawa⁶, A. Uritani⁷, and S. Goriely⁸

¹*Advanced Photon Research Center,*

Japan Atomic Energy Research Institute, Japan

²*Department of Physics, Konan University, Japan*

³*Strahlentherapie, Diakoniekrankehaus Schwäbisch Hall, Germany*

⁴*Institute of Advanced Energy, Kyoto University, Japan*

⁵*Cyclotron Institute, Texas A&M University, USA*

⁶*Photonics Research Institute,*

National Institute of Advanced Industrial Science and Technology, Japan

⁷*National Metrology Institute,*

National Institute of Advanced Industrial Science and Technology, Japan

⁸*Institut d'Astronomie et d'Astrophysique,*

Université Libre de Bruxelles, Belgium

(Dated: March 27, 2018)

Cross sections of the ^{186}W , ^{187}Re , $^{188}\text{Os}(\gamma, n)$ reactions were measured using quasi-monochromatic photon beams from laser Compton scattering (LCS) with average energies from 7.3 to 10.9 MeV. The results are compared with the predictions of Hauser-Feshbach statistical calculations using four different sets of input parameters. In addition, the inverse neutron capture cross sections were evaluated by constraining the model parameters, especially the $E1$ strength function, on the basis of the experimental data. The present experiment helps to further constrain the correction factor F_σ for the neutron capture on the 9.75 keV state in ^{187}Os . Implications of F_σ to the Re-Os cosmochronology are discussed with a focus on the uncertainty in the estimate of the age of the Galaxy.

PACS numbers: PACS number(s):25.20.-x,25.40.Lw,26.20.+f

I. INTRODUCTION

as

$$\frac{N_s(^{187}\text{Os})}{N_s(^{186}\text{Os})} \approx F_\sigma \frac{\langle \sigma \rangle(^{186}\text{Os})}{\langle \sigma \rangle(^{187}\text{Os})}. \quad (1)$$

Owing to the long half-life of ^{187}Re , the ^{187}Re - ^{187}Os pair may serve as a cosmochronometer to measure the duration of stellar nucleosynthesis that precedes the solidification of the solar system [1]. By adding the age of the solar system (~ 4.6 Gyr), it provides the age of the Galaxy. The facts that both ^{186}Os and ^{187}Os are produced only by the s-process nucleosynthesis apart from the cosmoradiogenic yield of ^{187}Os and that the isotopic solar abundance ratio of ^{186}Os and ^{187}Os [2] is available make this chronometer potentially reliable in the sense that it is independent of r-process models. The quantitative interpretation is, however, complicated by the possible enhancement of ^{187}Re - ^{187}Os transmutation rates in stellar condition, the stellar production and destruction of ^{187}Re and ^{187}Os during the chemical evolution of the Galaxy, the possible existence of s-process branchings at ^{185}W and ^{186}Re , and the neutron capture by the 9.75 keV first excited state in ^{187}Os [3, 4, 5, 6].

The last issue on the effect of neutron capture on the 9.75 keV state in ^{187}Os was raised in Ref. [6]. In the local approximation, the ratio of the s-process yields of ^{186}Os and ^{187}Os , $N_s(^{186}\text{Os})/N_s(^{187}\text{Os})$, can be expressed

Here, $\langle \sigma \rangle(^{186}\text{Os})$ and $\langle \sigma \rangle(^{187}\text{Os})$ are the Maxwellian-averaged neutron capture cross sections on ^{186}Os and ^{187}Os in the ground states, respectively. The F_σ value accounts for the correction to the cross section due to the neutron capture on the 9.75 keV state in ^{187}Os which is substantially populated at typical s-process temperatures $T \simeq 1\text{-}3 \times 10^8$ K. It is defined by

$$F_\sigma = \frac{\langle \sigma \rangle(^{187}\text{Os})}{\langle \sigma \rangle^*(^{187}\text{Os})} \quad (2)$$

with $\langle \sigma \rangle^*(^{187}\text{Os})$ being the Maxwellian-averaged neutron capture cross section on ^{187}Os at a given stellar temperature. Here, the first excited state in ^{186}Os and the second excited state in ^{187}Os lie at higher excitation energies of 137 keV and 74 keV, respectively, and therefore their contributions to neutron capture in the stellar condition may safely be ignored. In 1970s, it was of critical concern whether or not the F_σ value exceeds unity, because it has a great impact on the age of the Galaxy; the larger the F_σ , the smaller the age. However, there was a large spread in the early estimate (0.80-1.10 [6], 0.8 [7], and ~ 1.5 [8]).

This concern, combined with the fact that a direct measurement of neutron capture on the 9.75 keV state is virtually impossible, led to measurements of neutron capture on $^{186,187,188}\text{Os}$ [9, 10] and neutron inelastic scattering to the 9.75 keV state in ^{187}Os [11, 12]. The measured neutron capture cross sections were in good agreement with those of the earlier measurements [13, 14]. But, the statistical analysis of the capture data gave a lower bound of $0.30 b$ to the inelastic scattering cross section $\sigma_{nn'}$ at a neutron energy of 30 keV, and by combining with an upper limit of $\sigma_{nn'} = 0.5 b$ [15], gave $F_\sigma \sim 1$. In contrast, the two neutron inelastic scattering data, $\sigma_{nn'} = 1.13 \pm 0.2 b$ at 60 keV [11] and $1.5 \pm 0.2 b$ at 34 keV [12], are consistent with $F_\sigma = 0.80-0.83$ and 0.80 , respectively, within the statistical models.

More recent efforts have been made toward a unified statistical model analysis of all available data including measurements of (n, γ) cross sections [16] and elastic/inelastic scattering cross sections [17] on a neighboring nucleus ^{189}Os in which the ground state with $J^\pi = 3/2^-$ and the first excited state with $1/2^-$ at 36 keV appear in the reverse order of the corresponding states in ^{187}Os . These analyses showed that $F_\sigma = 0.79-0.83$.

In the Hauser-Feshbach statistical model calculations, however, large uncertainties may arise from the γ -ray transmission coefficients rather than the neutron optical potential and the level density. Information on the γ -ray transmission coefficients for neutron captured states in the low-energy tail of the giant dipole resonance in ^{188}Os can be obtained in the inverse photo-disintegration of ^{188}Os . But, the conventional Lorentzian model based on the previous photo-disintegration data on ^{188}Os [18] may not be satisfactory for two reasons. One reason is that the data taken with γ -ray beams from the positron annihilation in flight exhibit non-vanishing cross sections even below the neutron threshold (see sec. III B). The non-vanishing cross sections may be attributed to contributions from the positron bremsstrahlung. The other is that microscopic models can predict the $E1$ γ strength function more reliably than the Lorentzian model.

Besides F_σ , the effect of the s-process branchings at ^{185}W and/or ^{186}Re was parameterized as F_b and investigated within the framework of the schematic s-process models [4]. More recently, neutron capture cross sections were measured for neighboring ^{185}Re and ^{187}Re nuclei to derive the statistical model parameters from a consistent systematics [19]. With the improved parameters for s-process analysis, a stellar model calculation for low-mass AGB stars showed that the local approximation was disturbed by the branchings at ^{185}W and ^{186}Re . However, the precise physical conditions of the AGB model need to be scrutinized before any definite conclusion on F_b is drawn. This is clearly beyond the scope of the present study. Instead, the relevant statistical parameters, particularly the $E1$ γ strength function, can further be improved by the photo-disintegration measurement on ^{186}W .

In the present study, we have measured photoneutron

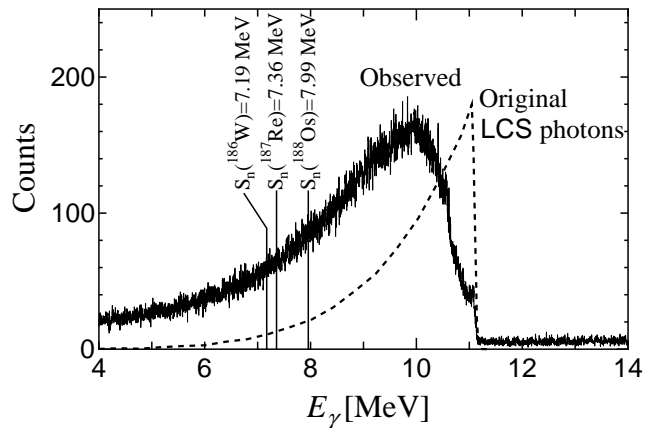


FIG. 1: An observed spectrum of the LCS photons measured with an HP-Ge detector (solid line). The original LCS photons simulated by the Monte Carlo code EGS4 is also shown with dashed line. The neutron separation energies S_n of ^{186}W , ^{187}Re and ^{188}Os are indicated by solid lines. Fractional photons with energies higher than S_n are responsible for the photoneutron reactions.

cross sections of ^{186}W , ^{187}Re and ^{188}Os using tunable quasi-monochromatic γ -ray beams from laser Compton scattering (LCS). The photo-disintegration data allow us to constrain F_σ values within the Hauser-Feshbach statistical model and discuss their implications to the Re-Os cosmochronology. Part of the present data has already been published [20].

II. EXPERIMENTAL PROCEDURE

Photoneutron cross section measurements on ^{186}W , ^{187}Re and ^{188}Os were performed at the National Institute of Advanced Industrial Science and Technology (AIST). Tunable quasi-monochromatic photon beams were generated by Compton scattering of laser photons, with relativistic electrons circulating in the storage ring TERAS [21]. A Nd:YLF Q-switch laser at a wavelength of 527 nm in second harmonics was operated at a frequency of 2 kHz. The electron energy was varied in the range from 450 to 588 MeV to produce LCS photons with the average energy from 7.3 and 10.9 MeV. A 20 cm lead collimator with a small hole of 2 mm in diameter was placed at approximately 6 m downstream from the interaction area which defines a scattering cone of the LCS photons. The typical energy resolution was 10 % in FWHM. Further details on the experimental setup can be found in Ref. [22].

Figure 1 shows an energy spectrum of the LCS photons measured by an HP-Ge detector with a relative efficiency of 120 %. The energy was calibrated at 1460.8 and 2614.5 keV with ^{40}K and ^{208}Tl radioactive isotopes of natural origin. A Monte Carlo simulation was performed with the EGS4 code [23] to analyze the response of the Ge detector. The energy distribution of incident

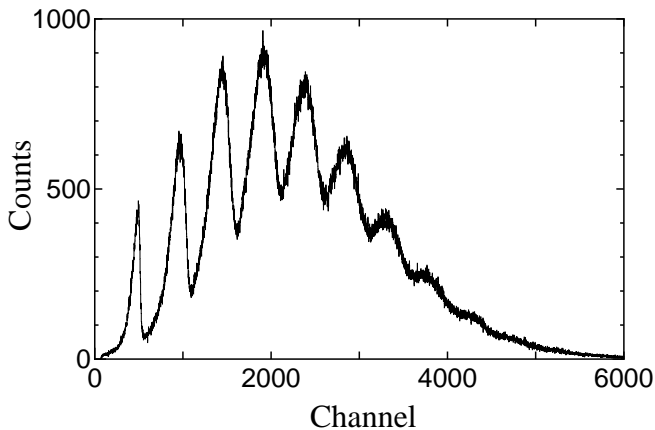


FIG. 2: Pile-up spectrum of the LCS photons measured with a large volume ($8'' \times 12''$) NaI(Tl) scintillation detector. In this spectrum the average photon number per laser pulse is 5.4 which leads to the LCS photon intensity of 1.08×10^4 /s.

LCS photons (dotted line in Fig. 1) was determined so as to reproduce the observed response function (solid line in Fig. 1). Photons with energies higher than the neutron threshold ($S_n=7.19$ MeV for ^{186}W , $S_n=7.36$ MeV for ^{187}Re and $S_n=7.99$ MeV for ^{188}Os) are responsible for the (γ, n) reactions. The fraction of these photons in the total photon flux and the average photon energy were obtained from the original LCS photon spectrum.

The beam current of the electron storage ring decreases exponentially in a normal condition with a lifetime ~ 6 hours. In the EGS4 Monte Carlo simulation, it was found that the electron beam size in the region of the interaction with laser photons varied with time: for example, from 2.2 mm in diameter at 166 mA to 1.2 mm at 72 mA in the ^{187}Re measurement. A space-charge effect is considered to be a main cause for the decrease in the beam size. This beam size effect, which was evident in long runs near the neutron thresholds, introduced uncertainties in the fraction of the LCS photon beam above the threshold. The resultant uncertainty was estimated to be 1 - 6 % in the present experiment. On the other hand, the average photon energy was determined well within 40 keV.

The number of LCS photons was monitored during the experiment using a large volume ($8'' \times 12''$) NaI(Tl) scintillation detector placed behind targets. A typical pile-up spectrum is shown in Fig. 2. The pulse height of the spectrum is proportional to the number of LCS photons per beam pulse. The photon flux was determined with 3 % uncertainty based on a statistical analysis on the pile-up spectrum [24].

Metallic powders of 1246 mg ^{186}W , 996 mg ^{187}Re , and 693 mg ^{188}Os enriched to 99.79, 99.52 % and 94.99 %, respectively, were pressed to self-supporting tablets with a diameter of 8 mm. The ^{188}Os powder included major contaminants of ^{189}Os (2.55 %), ^{190}Os (1.27 %) and ^{192}Os (0.97 %). These tablets were mounted inside thin containers made of aluminum, and were irradiated with the LCS photon beams. The threshold energy of the

(γ, n) reaction on ^{27}Al is 13.06 MeV, which is higher than those for ^{186}W , ^{187}Re and ^{188}Os . The present photoneutron cross section measurements were performed at energies below the threshold energy and therefore undisturbed by the $^{27}\text{Al}(\gamma, n)$ reaction. Further, measurements with an empty aluminum container (blank target) showed that no background neutrons were produced from photo-disintegration of possible impurities in the aluminum.

Emitted neutrons were detected by sixteen ^3He proportional counter (EURISYS MESURES 96NH45) embedded into a polyethylene moderator. Two sets of eight counters were placed in double concentric (inner and outer) rings at 7 and 10 cm from the beam axis. Time correlations (Fig. 3) between the neutron signal and the laser pulse were measured to estimate the number of background neutrons that arrived randomly at the ^3He detectors. These background neutrons were most likely produced by bremsstrahlung arising from collisions of electrons with residual gaseous molecules in the storage ring. In the moderation time distribution, constant events above 400 μs and at small correlation times were taken to be background neutrons. The constant background was further confirmed by using a 1 kHz laser and a wider (1 ms) time range (see, for example, Fig. 3 of Ref. [25]). The background subtraction is included in the statistical uncertainties through the error propagation.

The neutron detection efficiency was measured at the average neutron energy 2.14 MeV with a standard ^{252}Cf source. The dependence of the efficiency on neutron energy was determined by a Monte Carlo MCNP simulation with the statistical accuracy less than 0.5 % [25]. The so-called ring ratio between the count rates of inner and outer rings was used to determine the average energy of emitted neutrons [22]. A polynomial fit to the energy dependence of the ring ratios was made as in [22], where an asymptotic value of the ring ratio (8.0) at 10 keV simulated for the present neutron detector [25] was used as a constraint. The ring ratio varied between 7.4 and 2.9, indicating the neutron energies of several tens to a few hundreds keV for measurements close above the thresholds and up to 0.82 MeV at higher photon energies. The uncertainty in the neutron energy thus determined was estimated to be 10-15 keV, resulting in the uncertainty less than 0.8 % in the total neutron detection efficiency. Note that the total efficiency is nearly constant (44.4-44.3 %) over the neutron energy from 1 MeV to 400 keV and that it slowly decreases to 39.5 % at 50 keV. The overall systematic uncertainty for cross sections was estimated to be 5.9-8.3 %, which was determined by the neutron emission rate of the calibration source (5 %), the number of the incident LCS photons (3 %), and the beam size effect.

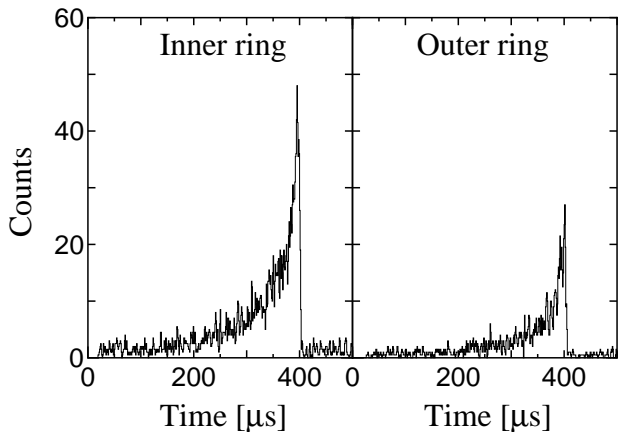


FIG. 3: Typical time-correlated spectra between laser pulses and neutrons detected in the inner (left panel) and outer (right panel) rings. The time correlation was measured by using a TAC module with the neutron signal and the 2 kHz laser pulse being the start and stop, respectively.

III. RESULTS

A. Data reduction

The photoneutron cross section measured with a monochromatic photon beam is given by

$$\sigma = \frac{n_n}{N_t N_\gamma f \epsilon_n(E_n)} \quad (3)$$

where n_n is the number of neutrons detected with the ^3He counters, N_t is the number of target nuclei per unit area, N_γ is the number of incident photons, f is the correction factor for a thick-target measurement, and $\epsilon(E_n)$ is the neutron detection efficiency. The correction factor is given by $f = (1 - e^{-\mu d})/(\mu d)$ with the linear attenuation coefficient of photons, μ , and the target thickness, d . The attenuation coefficient was taken by interpolation from [26] for the average energy of the LCS photons. The energy spread of the LCS photon beam in the full-width at half maximum makes negligible contributions ($\lesssim 0.2\%$) to the determination of the correction factor f , which deviates from unity by no more than 6% in the present measurements.

Recently, a methodology was developed to determine cross sections for reactions induced by a quasi-monochromatic photon beam [20]. When the photon beam has an energy distribution of $n_\gamma(E)$, $N_\gamma \sigma$ in Eq. (3) has to be replaced by the integral $\int n_\gamma(E) \sigma(E) dE$. By expanding the cross section $\sigma(E)$ in the Taylor series at the average photon energy E_0 , the first term in the Taylor series $\sigma(E_0)$ (the cross section at the average energy) was numerically evaluated along with the higher-order terms. The new methodology determines $\sigma(E_0)$ in the energy region of astrophysical importance near threshold within 6% corrections from the monochromatic approxi-

mation (Eq. (3)). Photoneutron cross sections presented in this paper are based on this methodology.

B. Photoneutron cross sections

Photoneutron cross sections measured for ^{186}W , ^{187}Re and ^{188}Os are shown in Fig. 4 and Table I. The contributions from the reactions with the main contaminants (^{189}Os , ^{190}Os and ^{192}Os) of the ^{188}Os target were estimated from the previous data from Ref. [27]. The error bars in Fig. 4 include both the statistical and systematic uncertainties. Previously, cross section data were taken for ^{186}W [18] and ^{188}Os [27] with quasi-monochromatic photons from positron annihilation in flight, as shown in Fig. 4 for comparison. In addition, data for ^{186}W and ^{187}Re were taken with bremsstrahlung [28, 29, 30]. In Ref. [30], yield curves obtained in small increments of the electron beam energy with 1-MeV spacing were converted to cross sections through an unfolding procedure based on the Penfold-Leiss method [31]. As mentioned in Ref. [30], it is a known fact [32] that cross sections are not obtained correctly because of *swings* of the solution, though uncertainties resulting from the swings may be reduced significantly.

The present ^{188}Os data are in reasonable agreement with the previous data [27] except at the low energy where the previous data exhibit non-vanishing cross sections even below the neutron threshold of 7.99 MeV. The non-vanishing cross sections may be attributed to *left-over* in the subtraction of contributions of the positron bremsstrahlung admixed with the positron annihilation photons.

The (γ, n) cross section exhibits the threshold behavior [33, 34] of

$$\sigma(E) = \sigma_0 \left(\frac{E_\gamma - S_n}{S_n} \right)^p. \quad (4)$$

Here, p is related to the neutron orbital angular momentum ℓ through $p = \ell + 1/2$. The values of $p = 0.5$ and 1.5 are expected for the s- and p-wave neutron decays, respectively. The best fits to the present experimental data gave $p = 0.47$ and $\sigma_0 = 78$ mb for the $^{186}\text{W}(\gamma, n)$ reaction, $p = 0.67$ and $\sigma_0 = 117$ mb for the $^{187}\text{Re}(\gamma, n)$ reaction, and $p = 0.53$ and $\sigma_0 = 143$ mb for the $^{188}\text{Os}(\gamma, n)$ reaction. The results show a rather pure s-wave character for the ^{186}W and $^{188}\text{Os}(\gamma, n)$ reactions, and suggest an admixture of p- and/or d-wave neutron emissions following the $E1$ excitation of ^{187}Re . The cross-section parametrization (Eq. (4)) was also made in the bremsstrahlung measurements [28, 29]; the results are in rough agreement with our new experimental data.

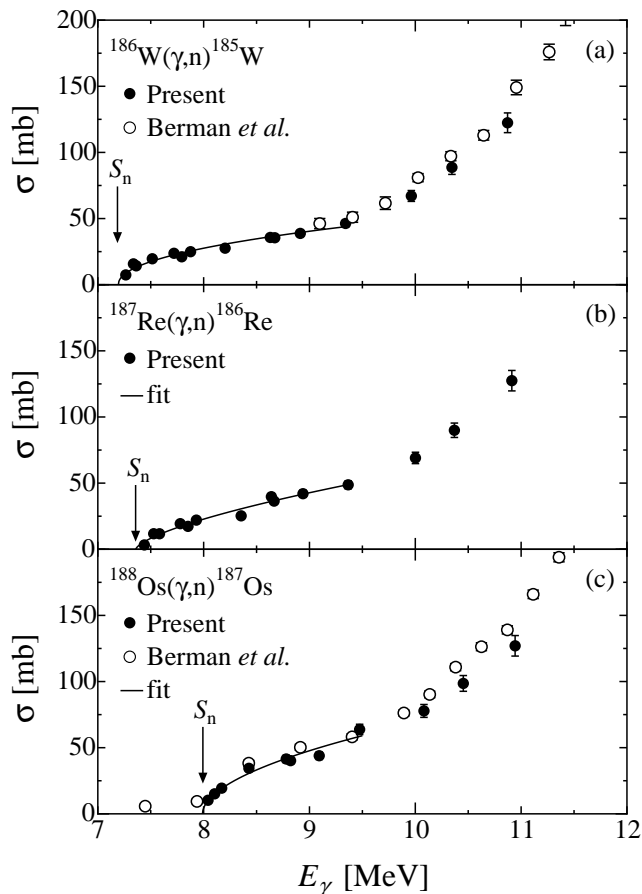


FIG. 4: Photoneutron cross sections of the reactions $^{186}\text{W}(\gamma, n)^{185}\text{W}$ (a), $^{187}\text{Re}(\gamma, n)^{186}\text{Re}$ (b), and $^{188}\text{Os}(\gamma, n)^{187}\text{Os}$ (c) extracted from the present data are plotted with filled circles. The previous data for ^{186}W [18] and ^{188}Os [27] taken with quasi-monochromatic photon beams are also shown with open circles for comparison. Given with solid line is the best fits to the experimental data in Eq. 4.

IV. COMPARISON WITH THEORY

A. Theoretical framework

The cross sections measured in the present work are now compared with the predictions of the Hauser-Feshbach (HF) compound nucleus theory [7, 35]. The uncertainties involved in HF cross section calculation are known not to be related to the theory of compound nucleus emission itself, but rather to the uncertainties associated with the evaluation of the nuclear properties entering the calculation of the transmission coefficients. It is therefore of prime importance to compare the effects of different nuclear inputs to estimate the reliability and accuracy of the predictions, especially when considering the reverse rates, i.e. in the present case, the radiative neutron capture rate which might be sensitive to different input parameters than the rate measured. In the present work, the nuclear level densities are derived from

TABLE I: Photoneutron cross sections of the reactions $^{186}\text{W}(\gamma, n)^{185}\text{W}$, $^{187}\text{Re}(\gamma, n)^{186}\text{Re}$, and $^{188}\text{Os}(\gamma, n)^{187}\text{Os}$. $E_{\text{ph}}^{\text{av}}$ is the average energy of the LCS photon beam. Cross sections are given as $\sigma \pm \Delta\sigma(\text{stat.}) \pm \Delta\sigma(\text{syst.})$ in units of mb where $\Delta\sigma(\text{stat.})$ and $\Delta\sigma(\text{syst.})$ represent the statistical and systematic uncertainties.

Nucleus	$E_{\text{ph}}^{\text{av}}$ (MeV)	σ (mb)	$\Delta\sigma(\text{stat.})$ (mb)	$\Delta\sigma(\text{syst.})^a$ (mb)
^{186}W	7.26	7.40	1.35	0.43
	7.33	15.7	1.1	1.0
	7.36	14.3	0.5	0.9
	7.51	19.6	0.6	1.1
	7.72	23.7	0.7	1.4
	7.79	21.1	0.8	1.3
	7.88	25.0	0.6	1.5
	8.20	27.6	0.9	1.6
	8.63	35.7	0.8	2.1
	8.67	35.5	0.9	2.1
	8.91	38.8	0.7	2.3
	9.34	46.3	0.8	2.7
	9.96	67.1	1.3	3.9
	10.35	88.7	1.2	5.2
10.87	122	2	7	
^{187}Re	7.44	3.27	1.46	0.21
	7.53	11.7	0.8	0.7
	7.58	11.7	0.7	0.7
	7.78	19.3	0.8	1.3
	7.85	17.3	0.9	1.0
	7.93	22.0	0.8	1.3
	8.35	25.3	0.8	1.5
	8.64	39.8	0.9	2.3
	8.67	36.4	1.0	2.1
	8.94	42.0	1.1	2.4
9.37	48.7	0.9	2.8	
10.00	69.0	1.5	4.0	
10.37	90.0	1.4	5.2	
10.91	127	2	7	
^{188}Os	8.04	10.2	1.5	0.9
	8.10	15.1	1.6	1.0
	8.17	19.4	1.1	1.2
	8.43	34.4	1.2	2.0
	8.78	41.5	1.3	2.5
	8.82	40.2	1.2	2.3
	9.09	43.9	1.1	2.6
	9.47	63.8	1.1	3.7
	10.08	77.8	1.8	4.5
	10.45	98.6	1.6	5.8
10.94	127	2	7	

^a The uncertainty includes those associated with the neutron detection efficiency (5 %), the photon flux (3 %), and the beam size effect (1 - 6 %) added in quadrature.

two models, either the widely used back-shifted Fermi gas (BSFG) model based on the global parametrization of [36] or the microscopic calculations taking into account the discrete structure of the single-particle spectra associated with Hartree-Fock+BCS (HFBCS) potentials [37]. This model has the advantage of treating

shell, pairing and deformation effects consistently, and for practical applications, has been renormalized on existing experimental information (low-lying levels and s-wave neutron resonance spacings whenever available as in the cases considered here). The transmission coefficients for particle emission is calculated either with the so-called JLMB semi-microscopic potential of [38] derived from the Brückner–Hartree–Fock approximation based on a Reid’s hard core nucleon–nucleon interaction, or with the global phenomenological mass- and energy-dependent potential of Woods-Saxon type developed by [39].

The photon transmission function of particular interest in photoemission data is calculated assuming the dominance of dipole transitions in the photon channel. The electric- and magnetic-dipole (GDR) transition strength functions are usually described by a Lorentz-type function where the energies and widths are determined by experimental data, whenever they exist, or by appropriate parametrizations. However, the calculation of the radiative capture or photoabsorption at low energies (and particularly in stellar conditions where the excited states of the target nucleus are thermally populated) is particularly sensitive to the low-energy tail of the GDR of the compound system. The shape of the GDR is expressed most frequently by a generalized energy-dependent-width Lorentzian function adjusted on low-energy data [40]. To test such models, we consider here the Hybrid model [41] which couples the GDR Lorentzian description at high energies with an analytical approximation to the theory of finite Fermi systems at energies below the neutron separation energy [42].

In addition to the Hybrid model [41], the Quasi-Particle Random Phase Approximation (QRPA) model of [43] is also considered here for estimating the photon transmission coefficients. These QRPA calculations are self-consistently built on a ground state derived with the HFBCS approximation. The final $E1$ -strength functions is obtained by folding the QRPA strength with a Lorentzian function to account for the damping of collective motions and the deformation effects. This global calculation based on the SLy4 Skyrme interaction has been shown to reproduce relatively well photoabsorption and average resonance capture data at low energies [22, 43]. Note that both the Hybrid and QRPA models differ not only in the predictions of the position and width of the GDR, but also in the energy dependence of its tail, which is an important quantity to derive the reaction rate. Since we are here mainly concerned with the GDR tail at low energies and the prediction of the reverse neutron capture cross section, both $E1$ -strength functions are renormalized on the available experimental information on the position of the GDR peak and the corresponding maximum absorption cross section. In the case of the HFBCS+QRPA model, this adjustment is achieved within the folding procedure introduced to account for damping and deformation effects.

B. Comparison between experimental and theoretical rates

The final nuclear inputs considered in the present analysis are summarized in Table II. Four different sets are used to estimate the photoemission cross section as well as the reverse radiative neutron capture cross sections. The comparison between these 4 sets allow us to estimate the sensitivity of the cross sections to the various input quantities, but also the uncertainties affecting the final prediction of the neutron capture rate of astrophysical interest. In Fig. 5, our new experimental data are compared with the theoretical photoemission cross sections. Also shown are previous measurements obtained in the vicinity of the GDR peak energy [27, 30]. Most of the calculations agree relatively well with experimental data, down to energies close to the neutron threshold. The neutron optical potential and nuclear level densities influence the photoneutron cross section only in a small energy range of no more than 1 MeV above the neutron threshold, so that the global behavior of cross section is almost entirely dictated by the $E1$ -strength. Some specific comments can be made for each reaction:

- In the $^{186}\text{W}(\gamma, n)^{185}\text{W}$ case, the HFBCS+QRPA model predicts some extra strength at energies around 7.5-10 MeV with respect to the Hybrid model. This extra strength is clearly seen experimentally below 8 MeV but not above. However, all models overestimate the 7mb cross section at $E = 7.26$ MeV.
- In the case of the $^{187}\text{Re}(\gamma, n)^{186}\text{Re}$ reaction, the low-energy data can only be reproduced when adopting the BSFG model of nuclear level densities. The microscopic HFBCS-based model fails to describe the fast rise of the cross section at the neutron threshold. Around 11 MeV, the Hybrid and HFBCS+QRPA strength predict a relatively different cross section, the former one being compatible with the Goryachev et al. [30] and the later with our more accurate measurements.
- As far as $^{188}\text{Os}(\gamma, n)^{187}\text{Os}$ is concerned, all HF calculations reproduce relatively well the data, though the Hybrid model gives a lower cross section in the 8.5-10 MeV energy range.

C. Determination of the neutron capture cross sections

We now estimate the stellar Maxwellian-averaged neutron capture cross section $\langle\sigma\rangle^*$ of astrophysics interest on the basis of the calculations presented above, i.e constrained by the reverse photo-disintegration rate compatible with the new measurements. It should be recalled that the neutron capture cross section at energies of a

TABLE II: Overview of the 4 sets of nuclear ingredients adopted in the Hauser-Feshbach calculations.

Label	Level density	γ -strength	Optical potential
INP-1	HFBCS [37]	HFBCS+QRPA [43]	JLMB [38]
INP-2	BSFG [36]	HFBCS+QRPA [43]	JLMB [38]
INP-3	BSFG [36]	HFBCS+QRPA [43]	Woods-Saxon [39]
INP-4	BSFG [36]	Hybrid model[41]	JLMB [38]

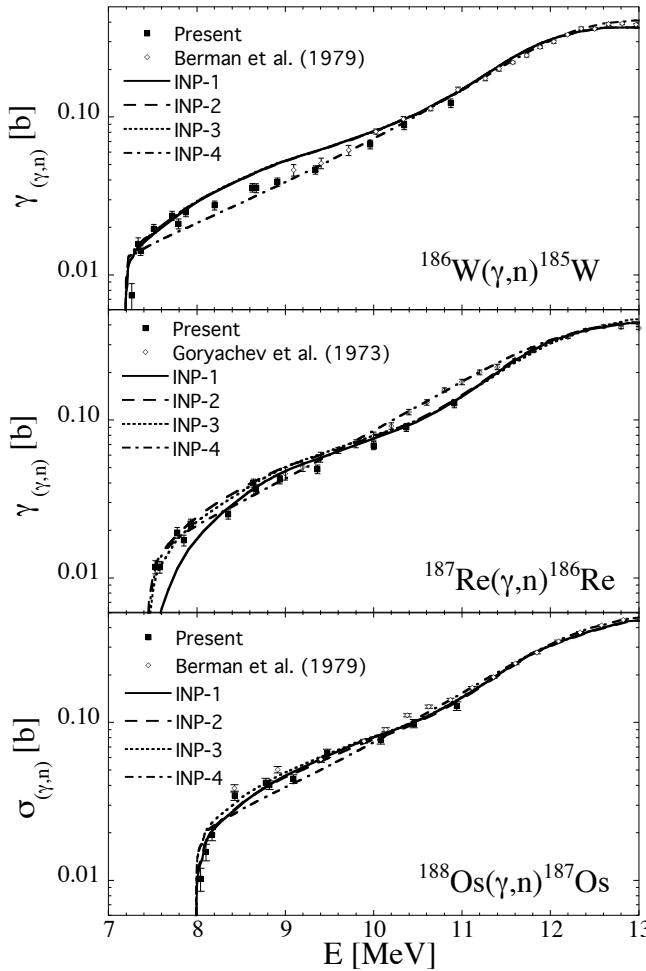


FIG. 5: Comparison between measured and calculated photoneutron cross sections for $^{186}\text{W}(\gamma, n)$ (upper panel), $^{187}\text{Re}(\gamma, n)$ (middle panel) and $^{188}\text{Os}(\gamma, n)$ (lower panel). The different theoretical predictions correspond to the input defined in Table II.

few tens of keV is mainly sensitive to photon transmission coefficient at an energy close to and even below the neutron separation energy. For this reason, only the calculations that reproduce the photoemission rate at the neutron separation energy relatively well are retained.

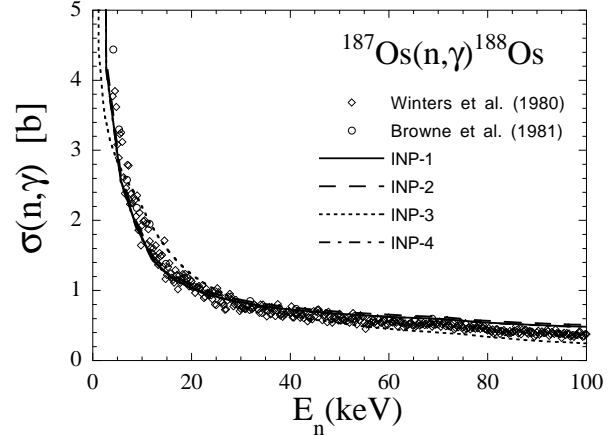


FIG. 6: Comparison between calculated and measured (open diamonds from [9] and open circles from [14]) neutron capture cross sections on ^{187}Os .

This leads us to reject the calculation ‘INP-1’ for the $^{187}\text{Re}(\gamma, n)^{186}\text{Re}$ reaction.

In the particular case of the stable ^{187}Os target, direct experimental data are available for the $^{187}\text{Os}(n, \gamma)^{188}\text{Os}$ reaction [9, 14] and used as additional constraints on the nuclear ingredients, namely the combination of the nuclear level density and optical potential. The resulting cross sections obtained with the 4 sets of nuclear inputs given in Table II are shown in Fig. 6 and seen to agree relatively well with experimental data, except in the specific ‘INP-3’ calculation where the use of the global optical potential [39] give rise to a cross section with an energy dependence relatively different from the one measured.

The stellar Maxwellian-averaged neutron capture cross sections for the three reactions studied here are shown in Fig. 7. It is evident that although the photoneutron cross section is relatively insensitive to the nuclear level density and neutron-nucleus optical potential, particularly in the $^{186}\text{W}(\gamma, n)^{185}\text{W}$ case, these quantities can affect the reverse rate significantly. If we characterize the remaining uncertainty affecting the prediction of the neutron capture rate by the ratio between the upper and lower limits obtained in Fig. 7, we find at an energy of 25 keV a factor of 1.9 for the $^{185}\text{W}(n, \gamma)^{186}\text{W}$ reaction, of 2.1 for $^{186}\text{Re}(n, \gamma)^{187}\text{Re}$ and only 1.1 for $^{187}\text{Os}(n, \gamma)^{188}\text{Os}$. In the last case, the small error bars arise from the additional constraints made available through the experimental $^{187}\text{Os}(n, \gamma)^{188}\text{Os}$ cross section.

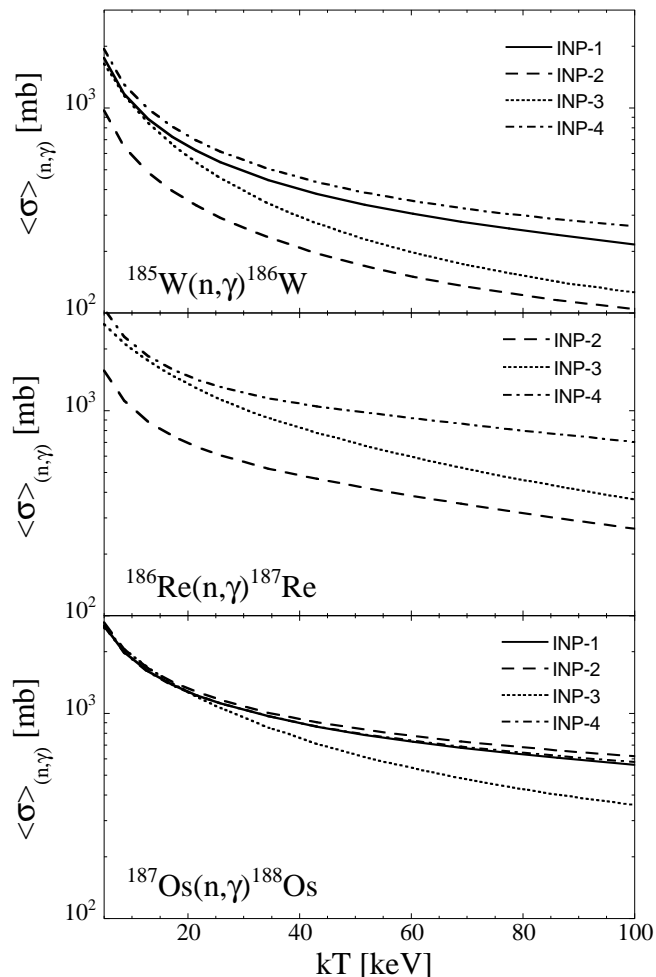


FIG. 7: Stellar Maxwellian-averaged neutron capture cross sections for ^{185}W (upper panel), ^{186}Re (middle panel), and ^{187}Os (lower panel) calculated on the basis of the HF input defined in Table II.

V. IMPLICATIONS TO THE RE-OS CHRONOMETRY

At stellar temperatures relevant to the s-process nucleosynthesis ($T \simeq 1-3 \times 10^8$ K), the ^{187}Os first excited state at 9.75 keV is strongly populated and can significantly affect the estimate of the stellar neutron capture rate on ^{187}Os . The correction to the cross sections due to the neutron capture on the 9.75 keV state is introduced by F_σ in Eq. (2).

On the basis of the present photoneutron data and the calculations, the temperature dependence of the F_σ factor has been re-estimated (Fig. 8 and Table III). At the s-process temperature of 3×10^8 K, all calculations converge to the F_σ value of about 0.87. However, at lower temperatures, the model INP-3 based on the global phenomenological optical potential predicts significantly larger F_σ values. This difference mainly originates from deviations seen in the laboratory cross section (cf. Fig. 6) and should therefore be given a lower credibility. The

TABLE III: Comparison between the F_σ values obtained in the present work (including INP-3 calculation) and those of Ref. [7] for different temperatures kT (expressed in keV).

kT	Present	Ref.[7]
12	0.901 – 0.937	0.867
20	0.879 – 0.886	0.839
25	0.866 – 0.874	0.830
30	0.859 – 0.867	0.820
52	0.822 – 0.847	0.813

present calculation agrees relatively well with the value of $0.80 \leq F_\sigma \leq 0.83$ at $kT=30$ keV from Ref. [11], but not with the value of $1 \leq F_\sigma \leq 1.15$ from Ref. [10].

We now consider implications of the F_σ values constrained by the present study to the Re-Os cosmochronology. The most tantalizing aspect of the Re-Os chronology is that it requires a rather detailed model of the chemical evolution of the Galaxy. Since constructing a reasonable model of the Galactic chemical evolution is beyond the scope of the present study, we rather focus on the uncertainty in the estimate of the age of the Galaxy within a schematic model.

We recall here that abundances of elements in the relevant mass region can be symbolically expressed as follows:

$$\begin{aligned}
 {}^{186}\text{Os}^\odot &= {}^{186}\text{Os}^s + {}^{186}\text{Os}^p \\
 {}^{187}\text{Os}^\odot &= {}^{187}\text{Os}^s + {}^{187}\text{Os}^c \\
 {}^{187}\text{Re}^\odot &= {}^{187}\text{Re}^r + {}^{187}\text{Re}^s - {}^{187}\text{Re}^c \\
 {}^{187}\text{Os}^c &= {}^{187}\text{Re}^c
 \end{aligned}$$

Here, \odot , s , p , r , and c represent the solar, s-process, p-process, r-process, and cosmoradiogenic origins, respectively. We introduce the following approximations:

$$\begin{aligned}
 {}^{186}\text{Os}^p &= p \times {}^{186}\text{Os}^\odot \\
 {}^{187}\text{Re}^s &= 0 \\
 {}^{187}\text{Os}^s &= [F_\sigma \langle \sigma \rangle ({}^{186}\text{Os}) / \langle \sigma \rangle ({}^{187}\text{Os})] {}^{186}\text{Os}^s \quad (\text{local approximation: Eq. (1)})
 \end{aligned}$$

Following the recent p-process calculations [44], we estimated p as lying within the 0.01-0.04 range, being in agreement with $p=0.02$ [19]. As noted earlier, we ignore the possible s-process contribution to ^{187}Re through the branchings at ^{185}W and ^{186}Re .

Thus, the cosmoradiogenic component of ^{187}Os can be obtained as

$${}^{187}\text{Os}^c = {}^{187}\text{Os}^\odot - (1-p)[F_\sigma \langle \sigma \rangle ({}^{186}\text{Os}) / \langle \sigma \rangle ({}^{187}\text{Os})] {}^{186}\text{Os}^\odot. \quad (5)$$

A consideration of the simplest model of a closed system would lead us to the assumption that the evolution of ^{187}Re can be effectively described by

$$\frac{d{}^{187}\text{Re}(t)}{dt} = -\lambda_\beta^{eff} {}^{187}\text{Re}(t) + Y(t) \quad (6)$$

where λ_{β}^{eff} is the effective β -decay rate of ^{187}Re in consideration of some enhancement by *astration* from the laboratory decay rate of $\lambda_{\beta} = \ln 2 / (41.6 \text{ Gyr})$, whereas $Y(t)$ term represents the net r-process yield. As in Ref. [19], we adopt a simple form of $Y(t) = y \exp(-\lambda t)$ where λ is a free parameter. Thus, we have

$$^{187}\text{Re}(t) = \frac{y[e^{-\lambda_{\beta}^{eff} t} - e^{-\lambda t}]}{\lambda - \lambda_{\beta}^{eff}}. \quad (7)$$

Using $d^{187}\text{Os}^c(t)/dt = +\lambda_{\beta}^{eff} ^{187}\text{Re}(t)$, the abundance ratio between $^{187}\text{Os}^c(t)$ and $^{187}\text{Re}(t)$ can be obtained as

$$\frac{^{187}\text{Os}^c(t)}{^{187}\text{Re}(t)} = \frac{B}{A} \quad (8)$$

where

$$A = e^{-\lambda_{\beta}^{eff} t} - e^{-\lambda t} \quad (9)$$

$$B = [1 - e^{-\lambda_{\beta}^{eff} t}] - [1 - e^{-\lambda t}] \lambda_{\beta}^{eff} / \lambda. \quad (10)$$

The abundance ratio in Eq. (8) at 4.55 Gyr ago is matched with that from Eq. (5).

For the meteoritic abundance of cosmogenic $^{187}\text{Os}^c$ relative to $^{187}\text{Re}^{\odot}$, we used the following solar abundances [45]:

$$\begin{aligned} ^{187}\text{Re}^{\odot} / ^{186}\text{Os}^{\odot} &= 3.51 \pm 0.09 \\ ^{187}\text{Os}^{\odot} / ^{186}\text{Os}^{\odot} &= 0.793 \pm 0.001. \end{aligned}$$

The (n, γ) cross section ratios at s-process temperatures, $\sigma(^{186}\text{Os})/\sigma(^{187}\text{Os})$, were taken from Ref. [19]. Thus, the meteoritic quantity is determined with the present F_{σ} value being a unique parameter. As for $\lambda_{\beta}^{eff}/\lambda_{\beta}$ is used to calculate the abundance ratio in Eq. (8) at $t = T_G$ (the age of the Galaxy) -4.55 Gyr , Clayton [46] derived 1.4 from the work of Yokoi *et al.* [3], whereas more recent analyses suggest considerably lower values [47]. We adopt here 1.2 as our standard value for the net enhancement by *astration* of the ^{187}Re β -decay rate.

Matching conditions in $^{187}\text{Os}^c / ^{187}\text{Re}^{\odot}$ were investigated in the T_G range of 11 - 15 Gyr, showing good agreement with $0 \lesssim \lambda \lesssim 2 \text{ Gyr}^{-1}$. We summarize some conclusions obtained under the simplest assumption of r-process nucleosynthesis yields varying exponentially in time.

- F_{σ} values at typical s-process temperatures are in the range of 0.86-0.94 (Table III).
- The probable range of the differential coefficient dT_G/dF_{σ} is $-(5.0-12.8) \text{ Gyr}$.

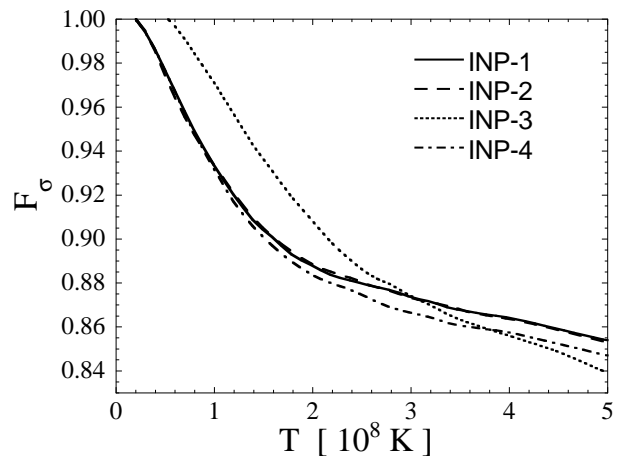


FIG. 8: Prediction of the F_{σ} factor on the basis of the different HF calculations defined in Table II and compared in Figs. 5 and 6 with experimental data.

- Consequently, the remaining uncertainty of T_G that stems from that of F_{σ} values is less than 1 Gyr. When the temperature dependence of $\langle \sigma \rangle(^{186}\text{Os}) / \langle \sigma \rangle(^{187}\text{Os})$ is considered along with that of F_{σ} , the uncertainty in T_G is approximately halved.

We note here that the model of Yokoi *et al.* [3] cannot be reconciled with the present F_{σ} data. The model of chemical evolution developed there favored F_{σ} values much higher than unity. If we mimic the results in terms of Eq. (6), the corresponding values of λ become negative. This also explains the much larger $|dT_G/dF_{\sigma}|$ values of up to 100 Gyr (as seen in the slope of Fig. 9 in Ref. [3]). Finally, it is noted that if we would use the age of the universe as derived by the WMAP ($T_U = 13.7 \pm 0.2 \text{ Gyr}$) [48], and assume $T_U - T_G \approx 1 \text{ Gyr}$, λ values that are consistent with the present F_{σ} value are narrowed in the ranges of 0.16-0.46 Gyr^{-1} , inclusively, and 0.22-0.34 Gyr^{-1} , exclusively. The exclusive values are commonly allowed in calculations with all possible combinations of kT , F_{σ} , and T_G .

VI. CONCLUSION

Photoneutron cross sections were measured with accuracy for ^{186}W , ^{187}Re and ^{188}Os using quasi-monochromatic photon beams from laser Compton scattering (LCS) at energies near the neutron thresholds. The cross sections were used to constrain the model parameters in the framework of the Hauser-Feshbach model. Four different sets of nuclear ingredients were adopted to estimate the photoneutron cross sections and the reverse radiative neutron capture cross sections. When no experimental data on the direct (n, γ) cross section is available, an accuracy of about a factor of 2 was achieved in the predictions. The influence of the neutron

capture by the 9.75 keV first excited state in ^{187}Os which is substantially populated in stellar plasmas at typical s-process temperatures has been estimated in connection with the ^{187}Re - ^{187}Os cosmochronology and shown to lead to an increase of the neutron capture rate by a factor of about 1.15 at a temperature of 3×10^8 K. Uncertainties by about 10% associated with the neutron-nucleus optical potential still affect the stellar rate at temperatures between 1 and 2×10^8 K.

The correction factor F_σ to be used in the local approximation (Eqs. (1) and (2)) was constrained well in the present study (Table III). Based on the simplest assumption of r-process nucleosynthesis yields varying exponentially in time, the cosmochronological uncertainty in the age of the Galaxy arising from the F_σ values is

estimated to be less than 1 Gyr; when the temperature dependences of both $\langle\sigma\rangle(^{186}\text{Os})/\langle\sigma\rangle(^{187}\text{Os})$ and F_σ are considered, the uncertainty is less than 0.5 Gyr.

Acknowledgments

H.U. is grateful to Kohji Takahashi for helpful suggestions. This work was done within the Konan-ULB joint project and supported by the Japan Atomic Energy Research Institute (the REIMEI Research Resource), the Japan Private School Promotion Foundation, and the Japan Society for the Promotion of Science. S.G. is FNRS Research Associate.

-
- [1] D.D. Clayton, *Astrophys. J.* **139**, 637 (1964).
 - [2] E. Anders and N. Grevesse, *Geochim. Cosmochim. Acta.* **53**, 197 (1989).
 - [3] K. Yokoi, K. Takahashi, and M. Arnould, *Astron. Astrophys.* **117**, 65 (1983).
 - [4] M. Arnould, K. Takahashi, and K. Yokoi, *Astron. Astrophys.* **137**, 51 (1984).
 - [5] K. Takahashi, *Nucl. Phys.* **A718**, 325c (2003).
 - [6] S.E. Woosley and W.A. Fowler, *Astrophys. J.* **233**, 411 (1979).
 - [7] J.A. Holmes, S.E. Woosley, W.A. Fowler, and B.A. Zimmerman, *Atomic Data and Nuclear Data Tables* **18**, 306 (1976).
 - [8] W.A. Fowler, in *Explosive Nucleosynthesis* ed. N.D. Schramm and W.D. Arnett (Austin: University of Texas Press 1973), p.300.
 - [9] R.R. Winters, R. L. Macklin, and J. Halperin, *Phys. Rev. C* **21**, 563 (1980).
 - [10] R.R. Winters and R.L. Macklin, *Phys. Rev. C* **25**, 208 (1982).
 - [11] R.L. Hershberger, R.L. Macklin, M. Balakrishnan, N.W. Hill, and M. T. McEllistrem, *Phys. Rev. C* **28**, 2249 (1983).
 - [12] R.L. Macklin, R.R. Winters, N.W. Hill, and J.A. Harvey, *Astrophys. J.* **274**, 408 (1983).
 - [13] J.C. Browne, G.P. Lamaze, and I.G. Schroder, *Phys. Rev. C* **14**, 1287 (1976).
 - [14] J.C. Browne and B.L. Berman, *Phys. Rev. C* **23**, 1434 (1981).
 - [15] R.R. Winters, F. Käppeler, K. Wisshak, B.L. Berman, and J.C. Browne, *Bull. Am. Phys. Soc.* **24**, 854 (1974).
 - [16] R.R. Winters, R.L. Maclin, and R.L. Hershberger, *Astron. Astrophys.* **171**, 9 (1987).
 - [17] M.T. McEllistrem, R.R. Winters, R.L. Hershberger, Z. Cao, R.L. Macklin, and N.W. Hill, *Phys. Rev. C* **40**, 591 (1989).
 - [18] B.L. Berman, M.A. Kelly, R.L. Bramblett, J.T. Caldwell, H.S. Davis, and S.C. Fultz, *Phys. Rev.* **185**, 1576 (1969).
 - [19] F. Käppeler, S. Jaag, Z. Y. Bao, and G. Reffo, *Astron. Astrophys.* **366**, 605 (1991).
 - [20] P. Mohr, T. Shizuma, H. Ueda, S. Goko, A. Makinaga, K. Y. Hara, T. Hayakawa, Y.-W. Lui, H. Ohgaki, and H. Utsunomiya, *Phys. Rev. C* **69**, 032801(R) (2004).
 - [21] H. Ohgaki, S. Sugiyama, T. Yamazaki, T. Mikado, M. Chiwaki, K. Yamada, R. Suzuki, T. Noguchi, and T. Tomimasu, *IEEE Trans. Nucl. Sci.* **38**, 386 (1991).
 - [22] H. Utsunomiya, H. Akimune, S. Goko, M. Ohta, H. Ueda, T. Yamagata, K. Yamasaki, H. Ohgaki, H. Toyokawa, Y.-W. Lui, T. Hayakawa, T. Shizuma, E. Khan, and S. Goriely, *Phys. Rev. C* **67**, 015807 (2003).
 - [23] W.R. Nelson, H. Hirayama, and W.O. Roger, *The EGS4 Code Systems*, SLAC-Report-265, (1985).
 - [24] H. Toyokawa, T. Kii, H. Ohgaki, T. Shima, T. Baba, and Y. Nagai, *IEEE Trans. Nucl. Sci.* **47**, 1954 (2000).
 - [25] K.Y. Hara, H. Utsunomiya, S. Goko, H. Akimune, T. Yamagata, M. Ohta, H. Toyokawa, K. Kudo, A. Uritani, Y. Shibata, Y.-W. Lui, and H. Ohgaki, *Phys. Rev. D* **68**, 072001 (2003).
 - [26] *Engineering Compendium on Radiation Shielding*, Vol. 1, *Shielding Fundamentals and Methods*, edited by R.G. Jaeger, E.P. Blizard, A.B. Chilton, M. Grotenhuis, A. Hönl, Th.A. Jaeger, and H.H. Eisenlohr (Springer-Verlag, New York, 1968), p.175.
 - [27] B.L. Berman, D.D. Faul, R.A. Alvarez, P. Meyer, and D.L. Olson, *Phys. Rev. C* **19**, 1205 (1979).
 - [28] K. Sonnabend, P. Mohr, K. Vogt, A. Zilges, A. Mengoni, T. Rauscher, H. Beer, F. Käppeler, and R. Gallino, *Astrophys. J.* **583**, 506 (2003).
 - [29] S. Müller, diploma thesis, Technische Universität Darmstadt, 2004 (unpublished).
 - [30] A.M. Goryachev, G.N.Zalesnyi, S.F. Semenko, and B.A. Tulupov, *Yad. Fiz.* **17**, 463 (1973).
 - [31] A.S. Penfold and J.E. Leiss, *Phys. Rev.* **114**, 1332 (1959).
 - [32] A.N. Tikhonov, *Dokl. Akad. Nauk SSSR* **151**, 501 (1963).
 - [33] E.P. Wigner, *Phys. Rev.* **73** (1948) 1002.
 - [34] G. Breit, *Phys. Rev.* **107**, 1612 (1958).
 - [35] W. Hauser and H. Feshbach, *Phys. Rev.* **87**, 366 (1952).
 - [36] S. Goriely, *J. Nucl. Science and Technology* (2002), Supp. 2 (Ed. K. Shibata), 536.
 - [37] P. Demetriou and S. Goriely, *Nucl. Phys.* **A695**, 95 (2001).
 - [38] E. Bauge, J.P. Delaroche, and M. Girod, *Phys. Rev. C* **63**, 024607 (2001).
 - [39] A.J. Koning and J.P. Delaroche, *Nucl. Phys.* **A713**, 231 (2003).
 - [40] J. Kopecky and M. Uhl, *Phys. Rev.* **C41**, 1941 (1990).

- [41] S. Goriely, Phys. Lett. **B436**, 10 (1998).
- [42] S.G. Kadenskii, V.P. Markushev, and V.I. Furman, Sov. J. Nucl. Phys. **37**, 165 (1983).
- [43] S. Goriely and E. Khan, Nucl. Phys. **A706**, 217 (2002).
- [44] M. Arnould and S. Goriely, Phys. Rep. **384**, 1 (2003).
- [45] T. Faestermann, Proc. 9th Workshop on Nuclear Astrophysics, 1998, ed. N. Hillebrandt and E. Müller, MPA/P12, p.172.
- [46] D.D. Clayton, Mon. Not. R. Astr. Soc. **234**, 1 (1988).
- [47] K. Takahashi, private communication.
- [48] D.N. Spergel, L. Verde, H.V. Peiris, E. Komatsu, M.R.olta, C.L. Bennett, M. Halpern, G. Hinshaw, N. Jarosik, A. Kogut, M. Limon, S.S. Meyer, L. Page, G.S. Tucker, J.L. Weiland, E. Wollack, and E.L. Wright, Astrophys. J. Supp. **148**, 175 (2003).